

Dark trions and biexcitons in WS_2 and WSe_2 made bright by e-e scattering

Mark Danovich¹, Viktor Zólyomi¹ & Vladimir I. Fal'ko¹

¹*National Graphene Institute, University of Manchester, Booth St E, Manchester M13 9PL, UK*

The direct band gap character and large spin-orbit splitting of the valence band edges (at the K and K' valleys) in monolayer transition metal dichalcogenides have put these two-dimensional materials under the spot-light of intense experimental and theoretical studies¹⁻⁷. In particular, for Tungsten dichalcogenides it has been found⁶⁻⁹ that the sign of spin splitting of conduction band edges makes ground state excitons radiatively inactive (dark) due to spin and momentum mismatch between the constituent electron and hole. One might similarly assume that the ground states of charged excitons and biexcitons in these monolayers are also dark. Here, we show that the intervalley ($K \rightleftharpoons K'$) electron-electron scattering mixes bright and dark states of these complexes, and estimate the radiative lifetimes in the ground states of these “semi-dark” trions and biexcitons to be ~ 10 ps, and analyse how these complexes appear in the temperature-dependent photoluminescence spectra of WS_2 and WSe_2 monolayers.

The truly 2D nature of TMDCs enhances the effects of Coulomb interaction^{10,11}, resulting in charge complexes such as excitons¹²⁻¹⁵, trions¹⁵ and biexcitons¹⁶ with binding energies that are orders of magnitude larger compared to conventional semiconductors such as GaAs. These complexes, which dominate the optical response of these materials, are comprised of spin/valley

polarised electrons and holes residing at the corners K and K' of the hexagonal Brillouin zone (BZ), where the selection rules of optical transitions require the same spin and valley states of the involved electrons at the conduction and valence band edges. As a result, the opposite spin projections of the conduction (c) and valence (v) band edges, found in monolayers of WS_2 and WSe_2 , makes ground state excitons in these 2D crystals dark⁹, so that their radiative transition would require help from defects, phonons¹⁷ or magnetic field^{18,19}.

Applying the spin and valley selection rules to ground state trions and biexcitons might imply that these charge complexes are dark, too. In the ‘dark’ (d) state both electrons are in the bottom spin-orbit split states of c -band, whereas in the state to be ‘bright’ (b), one of the electrons has to be in the excited spin-split state. Here, we show that an intervalley scattering^{20,21} of the c -band electrons mixes dark and bright states of complexes (Fig. 1), hence transferring some optical strength from b - to d -states and making dark state ‘semi-dark’. For the resulting recombination line of such semi-dark complexes, we find that it is shifted downwards in energy (relative to the bright exciton line) by $\sim 2\Delta_{SO}$, twice the c -band spin-orbit splitting.

With the reference to Fig. 1, the basis of trion, T (biexciton, B) states, $T_{\sigma_c\tau_c,\sigma_{c'}\tau_{c'}}^{\sigma_v\tau_v} (B_{\sigma_c\tau_c,\sigma_{c'}\tau_{c'}}^{\sigma_v\tau_v,\sigma_{v'}\tau_{v'}})$, can be described by spin, $\sigma = \uparrow, \downarrow$ and valley, $\tau = K, K'$ quantum numbers of their constituent c - and v -band states. In these notations, dark ground state exciton complexes $T_d (B_d)$ are $T_{\downarrow K', \uparrow K}^{\uparrow K}$ and $T_{\downarrow K, \uparrow K'}^{\downarrow K'}$ ($B_{\downarrow K, \uparrow K'}^{\uparrow K, \downarrow K'}$), and the excited states $T_{\uparrow K, \downarrow K'}^{\uparrow K}$ and $T_{\uparrow K, \downarrow K'}^{\downarrow K'}$ ($B_{\uparrow K, \downarrow K'}^{\uparrow K, \downarrow K'}$) are bright, $T_b (B_b)$ (Supplementary material S1). These states are mixed by the intervalley interaction illustrated by a

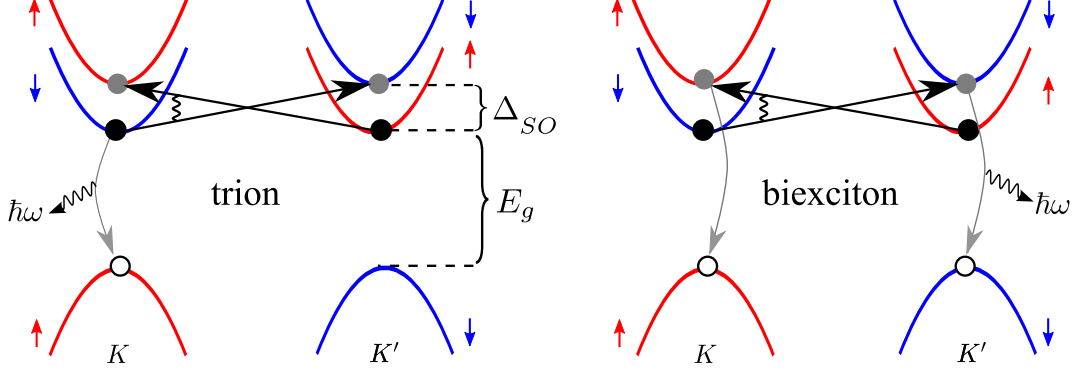


Figure 1 | Intervalley electron-electron scattering process.

Schematics of the band structures of WX_2 near the K, K' points of the BZ, and the intervalley scattering process that mixes dark and bright states of trions (T) and biexcitons (B). E_g is the band gap and Δ_{SO} stands for the conduction band spin splitting. Due to the large spin-orbit splitting in the valence band, the valence band is shown only for the higher-energy spin-polarised states.

sketch in Fig. 1,

$$H_{iv} = \frac{\hbar^2 \chi}{2m_c} \sum_{\sigma, \tau} \int d^2 \vec{r} \Psi_{c, \sigma, -\tau}^\dagger(\vec{r}) \Psi_{c, -\sigma, \tau}^\dagger(\vec{r}) \Psi_{c, -\sigma, -\tau}(r) \Psi_{c, \sigma, \tau}(\vec{r}). \quad (1)$$

Here, $\Psi_{c, \sigma, \tau}(\vec{r})$ are the conduction band electron field operators. The large momentum transfer between two electrons changing their valley states is determined by their Coulomb interaction at the unit cell scale, parametrised by a dimensionless factor χ . We estimate the size of this factor using both a tight-binding model and density functional theory (DFT). For the tight-binding model, we use the DFT calculated orbital decomposition to construct the Bloch states at the Brillouin zone corners, and we use a 3D Coulomb potential for the interaction between electrons. As the c -band states at the K/K' points are primarily composed^{6,7} of the metal $5d_{z^2}$ orbitals centred at the lattice sites \vec{R} of metallic atoms in TMDC lattice, $\phi(\vec{r} - \vec{R})$, which we use to construct the tight-binding

model Bloch states, to find

$$\chi = \frac{m_c}{m} \frac{A}{a_B} |C|^4 \sum_{\vec{R}} e^{i\vec{K}\cdot\vec{R}} \int d^3\vec{r}_1 d^3\vec{r}_2 \frac{|\phi(\vec{r}_1)|^2 |\phi(\vec{r}_2)|^2}{|\vec{r}_2 - \vec{r}_1 + \vec{R}|}. \quad (2)$$

Here, $\vec{K} = (\frac{4\pi}{3a_0}, 0)$ with a_0 the lattice constant of WX₂, $A = \frac{\sqrt{3}}{2}a_0^2$ is the unit cell area, m_c is the c -band electron effective mass, m is the free electron mass, a_B is the Bohr radius, and C is the transition metal $5d_{z^2}$ orbital amplitude in the c -band edge at the K point (Supplementary material S2.2). Similarly, we evaluated χ from wave functions obtained using DFT implemented in the local density approximation and VASP¹⁰ code (neglecting spin-orbit coupling). We used a plane-wave basis corresponding to 600 eV cutoff energy and a 12×12 grid of k -points in the 2D Brillouin zone. We also had to employ periodic boundary conditions in the z -direction; for this reason we used a large inter-layer distance of 20 Å to mimic the limit of an isolated monolayer. The form factor was calculated by post-processing the DFT wave functions, by taking the matrix element of the bare Coulomb interaction between the initial and final states of the scattering process (Supplementary material S2.1). These two calculations have returned values of the intervalley scattering factor χ , as listed in Table 2. In the basis of $[|d\rangle; |b\rangle]$ of dark and bright states of trions, $[T_{\downarrow K, \uparrow K'}^{\uparrow K}; T_{\uparrow K, \downarrow K'}^{\uparrow K}]$ and $[T_{\downarrow K, \uparrow K'}^{\downarrow K'}; T_{\uparrow K, \downarrow K'}^{\downarrow K'}]$, or biexcitons $[B_{\downarrow K, \uparrow K'}^{\uparrow K, \downarrow K'}; B_{\uparrow K, \downarrow K'}^{\uparrow K, \downarrow K'}]$, the coupling in Eq. (1) leads to the mixing

Table 1 | Material parameters.

Listed are the effective c - and v -band electron masses, c -band spin-orbit splitting, 2D screening length, bright exciton energy, trion binding energy, biexciton binding energy, and the velocity related to the off diagonal momentum matrix element.

	$\frac{m_c}{m}$ [7]	$\frac{m_v}{m}$ [7]	Δ_{SO} [7]	A [7]	r_* [15]	E_{X_b} [28]	ϵ_T [29]	ϵ_B [29]	$\frac{v}{c}$ [7]
			[meV]	[nm ²]	[nm]	[eV]	[meV]	[meV]	
WS ₂	0.26	-0.35	32	8.65	3.8	2	34	24	1.7×10^{-3}
WSe ₂	0.28	-0.36	37	9.38	4.5	1.7	31	20	1.6×10^{-3}

described by a 2×2 matrix

$$H = \begin{pmatrix} E_b^{T/B} & \mu_{T/B} \\ \mu_{T/B}^* & E_d^{T/B} \end{pmatrix}, \quad \mu_T = \frac{\hbar^2 \chi}{m_c} g_T, \quad \mu_B = \frac{\hbar^2 \chi}{m_c} g_B, \quad (3)$$

$$E_b^T = 2E_g + 2\Delta_{SO} - \epsilon_X - \epsilon_T + \delta',$$

$$E_d^T = 2E_g - \epsilon_X - \epsilon_T + \delta,$$

$$E_b^B = 2E_g + 2\Delta_{SO} - \epsilon_X - \epsilon_B + 2\delta',$$

$$E_d^B = 2E_g - \epsilon_X - \epsilon_B + 2\delta.$$

Where E_g is the band gap, ϵ_X , ϵ_T , and ϵ_B are the exciton, trion, and biexciton binding energies, respectively, and δ , δ' stand for the intravalley and intervalley electron-hole exchange²³, $\delta \approx 6$ meV, which we will neglect in the following calculations. Note that the effective masses of the c -band spin split bands differ by⁷ $\sim 30 - 40\%$ with the lower bands having the higher effective electron

mass. This results in slightly higher binding energies for the dark ground state charge complexes compared to the excited states, resulting in a larger value for their energy difference $E_b - E_d$. The mixing parameter $\mu \equiv \langle b|H_{iv}|d\rangle = \frac{\hbar^2\chi}{m_c} \int \prod_i d^2\vec{r}_i |\Phi_{T/B}|^2 \delta(\vec{r}_e - \vec{r}_{e'})$, (where $\Phi_{T/B}$ stands for the wave function of the trion or biexciton and $i = e, e', h, (h')$), is determined by the electron-electron contact pair densities²⁴ in the trion, g_T and biexciton, g_B .

The mixing of the dark and bright states results in a slight shift of their energies and, most importantly, in a finite radiative decay rate, τ_{sd}^{-1} of the semi-dark (sd) trions (T) and biexcitons (B),

$$\frac{1}{\tau_{sd}} \approx \left(1 - \frac{1}{\sqrt{1 + \left(\frac{\mu_{T/B}}{\Delta_{SO}}\right)^2}} \right) \frac{\alpha_{T/B}}{2} \tau_X^{-1}, \quad (4)$$

$$\frac{1}{\tau_X} = \frac{8\pi}{\hbar} \frac{e^2}{\hbar c} \frac{\hbar^2 v^2}{E_{X_b}} |\Phi_X(0)|^2,$$

where τ_X^{-1} is the radiative decay rate of the bright exciton^{25–27}, determined by the electron-hole overlap factor $|\Phi_X(0)|^2$ ($\Phi_X(r_{eh})$ is the envelope wave function describing relative motion of the electron and hole in the exciton), v is the velocity related to the off diagonal momentum matrix element. The values of the factors $\alpha_T = \frac{1}{2}$ and $\alpha_B = \frac{2}{3}$ have been estimated based on the following consideration. As the exciton's binding energy is significantly larger than that of the trion or biexciton, these bound complexes can be viewed as strongly-bound, with an additional weakly bound electron in the case of a trion, or an exciton in the case of a biexciton. For a trion, this results in a reduction of the recombining electron-hole contact pair density by a factor of 2, as the hole is shared between the two electrons such that the recombining electron (which has the right spin projection), will be near it only half of the time. In the case of the biexciton, the recombining

Table 2 | Radiative lifetimes and scattering matrix elements.

Listed are the Intervalley scattering parameter χ calculated using DFT and tight binding (TB) model and the corresponding trion and biexciton mixing parameters $\mu_{T/B}$ obtained using the electron-electron contact pair densities calculated in ref. 24 using quantum Monte Carlo, shown as DFT [TB], and the radiative lifetimes of the bright exciton, semi-dark trion and biexciton.

	χ_{DFT}	χ_{TB}	μ_T	μ_B	τ_X	$\tau_{sd}(T)$	$\tau_{sd}(B)$
			[meV]	[meV]	[ps]	[ps]	[ps]
WS ₂	1.0	1.6	18 [29]	13 [21]	0.25	7.7 [3.9]	10 [4.5]
WSe ₂	1.3	2.0	19 [30]	14 [22]	0.26	9.1 [4.7]	12 [5.7]

electron will be part of the time near the other hole and part of the time the other electron will be near the hole, giving a factor of 1/3, however in this case both holes can recombine radiatively with a proper electron producing an additional factor of 2, hence, giving $\alpha_B = \frac{2}{3}$. The resulting values for the lifetimes (using the material parameters in Table 1) are summarized in Table 2. The mixing of the dark and bright states produces photoluminescence lines shown schematically in Fig. 2. The emitted photon energies of these lines are determined by both the binding energies and the shake-up into the higher-energy spin-split *c*-band in the final state,

$$E_{X_b} = E_g + \Delta_{SO} - \epsilon_X, \quad (5)$$

$$E_{T_{sd}/B_{sd}} \approx E_{X_b} - \epsilon_{T/B} - 2\Delta_{SO},$$

$$E_{T/B} \approx E_{X_b} - \epsilon_{T/B}.$$

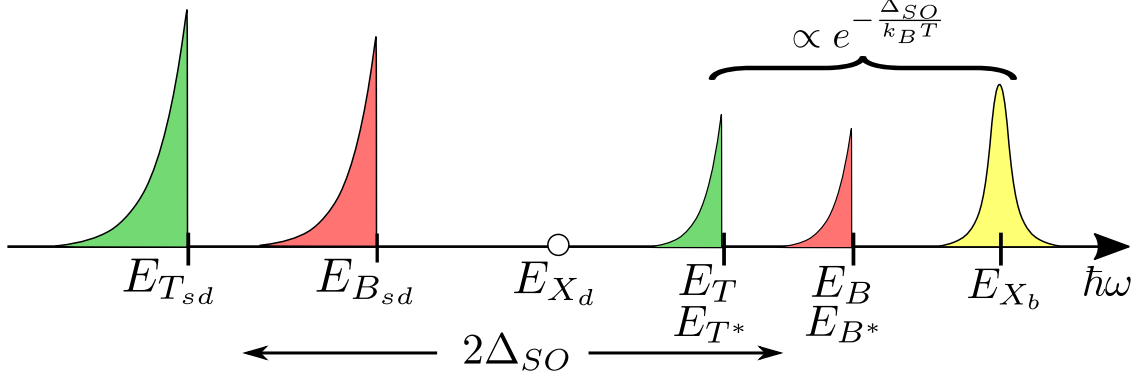


Figure 2 | Low temperature photoluminescence spectrum of WX_2 .

Sketch of the low temperature ($k_B T < \Delta_{SO}$) photoluminescence spectrum of WX_2 including the bright exciton, dark and bright trions (green) and dark and bright biexcitons (red). The excited bright trions and excitons are denoted by T^* and B^* . The dark exciton (X_d) energy is marked as a reference point $E_{X_d} = E_{X_b} - \Delta_{SO}$.

Being the ground states, the semi-dark trion and biexcitons (T_{sd}, B_{sd}) do not require an activation and therefore should appear in the spectrum even at low temperatures. In contrast, the bright states do require thermal activation, resulting in a $e^{-\Delta E/k_B T}$ temperature dependence of their lines intensities. For the bright exciton, trion $[T_{\uparrow K, \uparrow K'}^{\uparrow K}; T_{\downarrow K, \downarrow K'}^{\downarrow K'}]$ and biexciton $[B_{\uparrow K, \uparrow K'}^{\uparrow K, \downarrow K'}; B_{\downarrow K, \downarrow K'}^{\uparrow K, \downarrow K'}]$ we have $\Delta E \approx \Delta_{SO}$, while for the excited mixed dark and bright trion (T^*) $[T_{\uparrow K, \downarrow K'}^{\uparrow K}; T_{\uparrow K, \downarrow K'}^{\downarrow K'}]$ and biexciton (B^*) $B_{\uparrow K, \downarrow K'}^{\uparrow K, \downarrow K'}$, $\Delta E \approx 2\Delta_{SO}$. Also, the presence of a final state electron or exciton results in an antisymmetric line shape with a cutoff due to the recoil kinetic energy of the remaining electron or exciton that shifts the emission line to a lower energy. A typical recoil kinetic energy is $\frac{m_X}{m_c} k_B T$ for the trions and $k_B T$ for biexcitons, with k_B the Boltzmann constant, m_X the exciton mass, and m_c the c -band electron effective mass.

In conclusion, we have shown that intervalley electron-electron scattering makes “dark” ground state trions and biexcitons in Tungsten dichalcogenides WS_2 and WSe_2 optically active, with a lifetime $\tau_{T/B} \sim 10$ ps, to compare with a sub-ps lifetime of bright excitons in 2D TMDCs.

Acknowledgements The authors would like to thank I. Aleiner, T. Heinz, M. Potemski, M. Syniszewski, A. Tartakovski and X. Xu for useful discussions.

1. Qing Hua Wang, Kourosch Kalantar-Zadeh, Andras Kis, Jonathan N. Coleman, and Michael S. Strano. Electronics and optoelectronics of two-dimensional transition metal dichalcogenides. *Nat. Nanotechnol.*, 7(11):699–712, 11 2012.
2. Ting Cao, Gang Wang, Wenpeng Han, Huiqi Ye, Chuanrui Zhu, Junren Shi, Qian Niu, Pingheng Tan, Enge Wang, Baoli Liu, and Ji Feng. Valley-selective circular dichroism of monolayer molybdenum disulphide. *Nat. Commun.*, 3:887, 06 2012.
3. Di Xiao, Gui-Bin Liu, Wanxiang Feng, Xiaodong Xu, and Wang Yao. Coupled spin and valley physics in monolayers of MoS_2 and other group-vi dichalcogenides. *Phys. Rev. Lett.*, 108:196802, May 2012.
4. Aaron M. Jones, Hongyi Yu, Nirmal J. Ghimire, Sanfeng Wu, Grant Aivazian, Jason S. Ross, Bo Zhao, Jiaqiang Yan, David G. Mandrus, Di Xiao, Wang Yao, and Xiaodong Xu. Optical generation of excitonic valley coherence in monolayer wse_2 . *Nat Nano*, 8(9):634–638, 09 2013.

5. Hualing Zeng, Junfeng Dai, Wang Yao, Di Xiao, and Xiaodong Cui. Valley polarization in MoS₂ monolayers by optical pumping. *Nat Nano*, 7(8):490–493, 08 2012.
6. Gui-Bin Liu, Di Xiao, Yugui Yao, Xiaodong Xu, and Wang Yao. Electronic structures and theoretical modelling of two-dimensional group-vib transition metal dichalcogenides. *Chem. Soc. Rev.*, 44:2643–2663, 2015.
7. Andor Kormanyos, Guido Burkard, Martin Gmitra, Jaroslav Fabian, Viktor Zolyomi, Neil D Drummond, and Vladimir Fal'ko. k.p theory for two-dimensional transition metal dichalcogenide semiconductors. *2D Materials*, 2(2):022001, 2015.
8. J. P. Echeverry, B. Urbaszek, T. Amand, X. Marie, and I. C. Gerber. Splitting between bright and dark excitons in transition metal dichalcogenide monolayers. *Phys. Rev. B*, 93:121107, Mar 2016.
9. Xiao-Xiao Zhang, Yumeng You, Shu Yang Frank Zhao, and Tony F. Heinz. Experimental evidence for dark excitons in monolayer WSe₂. *Phys. Rev. Lett.*, 115:257403, Dec 2015.
10. Alexey Chernikov, Timothy C. Berkelbach, Heather M. Hill, Albert Rigosi, Yilei Li, Ozgur Burak Aslan, David R. Reichman, Mark S. Hybertsen, and Tony F. Heinz. Exciton binding energy and nonhydrogenic rydberg series in monolayer ws₂. *Phys. Rev. Lett.*, 113:076802, Aug 2014.
11. Pierluigi Cudazzo, Ilya V. Tokatly, and Angel Rubio. Dielectric screening in two-dimensional insulators: Implications for excitonic and impurity states in graphane. *Phys. Rev. B*, 84:085406, Aug 2011.

12. Kin Fai Mak, Keliang He, Changgu Lee, Gwan Hyoung Lee, James Hone, Tony F. Heinz, and Jie Shan. Tightly bound trions in monolayer mos₂. *Nat Mater*, 12(3):207–211, 03 2013.
13. Diana Y. Qiu, Felipe H. da Jornada, and Steven G. Louie. Optical spectrum of mos₂: Many-body effects and diversity of exciton states. *Phys. Rev. Lett.*, 111:216805, Nov 2013.
14. Ashwin Ramasubramaniam. Large excitonic effects in monolayers of molybdenum and tungsten dichalcogenides. *Phys. Rev. B*, 86:115409, Sep 2012.
15. Timothy C. Berkelbach, Mark S. Hybertsen, and David R. Reichman. Theory of neutral and charged excitons in monolayer transition metal dichalcogenides. *Phys. Rev. B*, 88:045318, Jul 2013.
16. Yumeng You, Xiao-Xiao Zhang, Timothy C. Berkelbach, Mark S. Hybertsen, David R. Reichman, and Tony F. Heinz. Observation of biexcitons in monolayer wse₂. *Nat Phys*, 11(6):477–481, 06 2015.
17. Mark Danovich, Viktor Zólyomi, Vladimir I Fal’ko, and Igor L Aleiner. Auger recombination of dark excitons in ws₂ and wse₂ monolayers. *2D Materials*, 3(3):035011, 2016.
18. Xiao-Xiao Zhang, Ting Cao, Zhengguang Lu, Yu-Chuan Lin, Fan Zhang, Ying Wang, Zhiqiang Li, James C. Hone, Joshua A. Robinson, Dmitry Smirnov, Steven G. Louie, Tony F. Heinz. Magnetic brightening and control of dark excitons in monolayer WSe₂. [cond-mat/1612.03558v1](https://arxiv.org/abs/cond-mat/1612.03558v1)

19. M. R. Molas, C. Faugeras, A. O. Slobodeniuk, K. Nogajewski, M. Bartos, D. M. Basko, M. Potemski. Brightening of dark excitons in monolayers of semiconducting transition metal dichalcogenides. *cond-mat/1612.02867v1*
20. Hongyi Yu, Xiaodong Cui, Xiaodong Xu, and Wang Yao. Valley excitons in two-dimensional semiconductors. *National Science Review*, 2(1):57–70, 2015.
21. Hanan Dery. Theory of intervalley coulomb interactions in monolayer transition-metal dichalcogenides. *Phys. Rev. B*, 94:075421, Aug 2016.
22. G. Kresse and J. Furthmüller. Efficient iterative schemes for *ab initio* total-energy calculations using a plane-wave basis set. *Phys. Rev. B*, 54:11169–11186, Oct 1996.
23. Gerd Plechinger, Philipp Nagler, Ashish Arora, Robert Schmidt, Alexey Chernikov, Andres Granados del Aguila, Peter C. M. Christianen, Rudolf Bratschitsch, Christian Schuller, and Tobias Korn. Trion fine structure and coupled spin-valley dynamics in monolayer tungsten disulfide. *Nat Commun*, 7, 09 2016.
24. Bogdan Ganchev, Neil Drummond, Igor Aleiner, and Vladimir Fal'ko. Three-particle complexes in two-dimensional semiconductors. *Phys. Rev. Lett.*, 114:107401, Mar 2015.
25. Maurizia Palummo, Marco Bernardi, and Jeffrey C. Grossman. Exciton radiative lifetimes in two-dimensional transition metal dichalcogenides. *Nano Letters*, 15(5):2794–2800, 2015.
26. A O Slobodeniuk and D M Basko. Spin–flip processes and radiative decay of dark intravalley excitons in transition metal dichalcogenide monolayers. *2D Materials*, 3(3):035009, 2016.

27. Haining Wang, Changjian Zhang, Weimin Chan, Christina Manolatou, Sandip Tiwari, and Farhan Rana. Radiative lifetimes of excitons and trions in monolayers of the metal dichalcogenide MoS_2 . *Phys. Rev. B*, 93:045407, Jan 2016.
28. A. T. Hanbicki, M. Currie, G. Kioseoglou, A. L. Friedman, and B. T. Jonker. Measurement of high exciton binding energy in the monolayer transition-metal dichalcogenides WS_2 and WSe_2 . *Solid State Communications*, 203:16–20, 2 2015.
29. Ilkka Kylänpää and Hannu-Pekka Komsa. Binding energies of exciton complexes in transition metal dichalcogenide monolayers and effect of dielectric environment. *Phys. Rev. B*, 92:205418, Nov 2015.

Supplementary material

S1 Group theory analysis of excitons, trions and biexcitons in Tungsten dichalcogenides

S1.1 Introduction

Group theory allows to utilize the symmetry properties of the Hamiltonian in order to gain insight into selection rules for microscopic processes in quantum systems. As a starting point, the eigenstates of the Hamiltonian are classified according to the irreducible representations (IrReps) of the symmetry group, in our case the point group C_{3h} . In monolayer TMDCs, DFT calculations^{1,2} (see also S2.1) have found that band edges of monolayer WS_2 and WSe_2 are found at the two inequivalent corners, K and K' of the Brillouin zone. Hence, for the sake of their classification we consider the extended point group^{3,4}, $C_{3v}'' = C_{3v} + tC_{3v} + t^2C_{3v}$, where t are translations by a lattice vector. This enables us to treat states of excitons and complexes at K , K' and zero momentum in the same fashion. The character table and product table for the IrReps of the extended point group C_{3v}'' are given in Tables S1, S2, respectively. DFT calculations^{1,2} (see also S2.1) have also found that at the K and K' valleys, the orbital composition of the Bloch states is dominated by the $z \rightarrow -z$ symmetric d -orbitals (d_0 for the c -band and $d_{\pm 2}$ for the v -band in the two valleys) of transition metal, allowing to classify the c and v -band Bloch states at the K and K' valleys as transforming

Table S1: C''_{3v} character table.

Character table for the irreducible representations (IrRep) of the extended point group C''_{3v} , and their correspondence to the conduction (c) and valence (v) band electrons states.

C''_{3v}	E	t, t^2	$2C_3$	$9\sigma_v$	$2tC_3$	$2t^2C_3$
A_1	1	1	1	1	1	1
A_2	1	1	1	-1	1	1
E	2	2	-1	0	-1	-1
$E'_1 (c)$	2	-1	-1	0	2	-1
$E'_2 (v)$	2	-1	2	0	-1	-1
E'_3	2	-1	-1	0	-1	2

according to the two dimensional IrReps of the extended point group, E'_1 and E'_2 , respectively.

Using classification of the single electron states, we consider excitons, trions, and biexcitons. For this, we take direct products of the corresponding IrReps, and, then, apply the product rules for the IrReps of C''_{3v} , shown in Table S2. This group theory analysis enables us to identify excitonic basis states that can be mixed by the intervalley e-e scattering, leading to the class of semi-dark trions and biexcitons discussed in the main text.

Table S2: C''_{3v} product table.

Product table for the irreducible representations of the extended point group C''_{3v} .

C''_{3v}	A_1	A_2	E	E'_1	E'_2	E'_3
A_1	A_1	A_2	E	E'_1	E'_2	E'_3
A_2	A_2	A_1	E	E'_1	E'_2	E'_3
E	E	E	$A_1 \oplus A_2 \oplus E$	$E'_2 \oplus E'_3$	$E'_1 \oplus E'_3$	$E'_1 \oplus E'_2$
$E'_1 (c)$	E'_1	E'_1	$E'_2 \oplus E'_3$	$A_1 \oplus A_2 \oplus E'_1$	$E \oplus E'_3$	$E \oplus E'_2$
$E'_2 (v)$	E'_2	E'_2	$E'_1 \oplus E'_3$	$E \oplus E'_3$	$A_1 \oplus A_2 \oplus E'_2$	$E \oplus E'_1$
E'_3	E'_3	E'_3	$E'_1 \oplus E'_2$	$E \oplus E'_2$	$E \oplus E'_1$	$A_1 \oplus A_2 \oplus E'_3$

S1.2 Excitons

The exciton states transform according to the direct product representation of the c - and v -band states given by

$$E'_1 \otimes E'_2 = E \oplus E'_3. \quad (\text{S6})$$

The 2D IrRep E corresponds to the intravalley excitons with both electron and hole residing in either the K or K' valleys, and the 2D IrRep E'_3 corresponds to the intervalley excitons with the electron and hole residing in opposite valleys making the exciton dark due to momentum mismatch. By further introducing the spin projections of the electron and hole, we have for each representation two possible total spin projections, $|S_z| = 1$ corresponding to dark excitons due to

spin conservation, and $S_z = 0$ corresponding to bright exciton states. Using the notation introduced in the text for trions and biexcitons, the E IrRep dark intravalley exciton states are given by $[X_{\downarrow K}^{\uparrow K}; X_{\uparrow K'}^{\downarrow K'}]$ with $|S_z| = 1$, and the bright intravalley excitonic states by $[X_{\uparrow K}^{\uparrow K}; X_{\downarrow K'}^{\downarrow K'}]$ with $|S_z| = 0$. Similarly, for the intervalley excitons transforming according to E'_3 , which are dark due to momentum conservation, we have $[X_{\uparrow K'}^{\uparrow K}; X_{\downarrow K}^{\downarrow K'}]$ with $S_z = 0$, and $[X_{\downarrow K'}^{\uparrow K}; X_{\uparrow K}^{\downarrow K'}]$ with $S_z = 1$, being dark due to both spin and momentum conservation.

S1.3 Trions

Next we classify the trion states composed of two electrons and a hole. The strongly bound trion states require the two-electron wave function to be symmetric with respect to exchanging the electrons coordinates and the two electrons to have different spin/valley indices corresponding to a singlet state, as obtained in ref. 5 using Monte Carlo calculations. The two-electron state transforms according to the direct product of the c -band electrons representations given by

$$E'_1 \otimes E'_1 = A_1 \oplus A_2 \oplus E'_1. \quad (\text{S7})$$

According to Table S1, the symmetric combination of the two electrons transforms according to A_1 or E'_1 . The identity representation corresponds to both electrons residing in opposite valleys, while the 2D IrRep E'_1 corresponds to both electrons residing in the same valley K or K' . Next, to obtain the representation of the trion we include the hole state E'_2 and take the direct product of the two electrons and the hole. This gives in the first case

$$A_1 \otimes E'_2 = E'_2, \quad (\text{S8})$$

corresponding to the hole residing in either the K or K' valleys and the electrons residing in opposite valleys. Including the spin projection this corresponds to the following trion states, $[T_{\downarrow K, \uparrow K'}^{\uparrow K}; T_{\downarrow K, \uparrow K'}^{\downarrow K}]$ which are the semi-dark singlet ground state trions, and $[T_{\uparrow K, \downarrow K'}^{\uparrow K}; T_{\uparrow K, \downarrow K'}^{\downarrow K'}]$ which are the excited bright trion singlet states. As the excited bright and semi-dark trion states both transform according to the same E'_2 IrRep, the two states can be mixed through the electron-electron intervalley scattering introduced in the main text, which transforms as the identity representation. The bright trion triplet states with both electrons in opposite valleys also transform according to the E'_2 IrRep and are given by $[T_{\uparrow K, \uparrow K'}^{\uparrow K}; T_{\downarrow K, \downarrow K'}^{\downarrow K'}]$, and the dark trion triplet states (due to spin conservation) are given by $[T_{\downarrow K, \downarrow K'}^{\uparrow K}; T_{\uparrow K, \uparrow K'}^{\downarrow K'}]$. In the second case, choosing for the two-electron representation the E'_1 IrRep,

$$E'_1 \otimes E'_2 = E \oplus E'_3. \quad (\text{S9})$$

Here, E corresponds to states with the two electrons and hole residing in the same valley K or K' . Requiring the electrons to have opposite spin projections gives the following bright trion states $[T_{\uparrow K, \downarrow K}^{\uparrow K}; T_{\uparrow K', \downarrow K'}^{\downarrow K'}]$. E'_3 corresponds to the two electrons residing in the same valley while the hole is in the opposite valley, giving the dark trion states (due to momentum conservation) $[T_{\uparrow K, \downarrow K}^{\downarrow K'}; T_{\uparrow K', \downarrow K}^{\uparrow K}]$.

S1.4 Biexcitons

The bound biexciton states are composed of a spatially symmetric wave function for the two electrons and for the two holes. This corresponds to the IrReps $A_1 \oplus E'_1$ for the two electrons, and

$A_1 \oplus E'_2$ for the two holes. Taking the direct product of the two-electron and two-hole states gives the possible representations of the biexciton states

$$(A_1 \oplus E'_1) \otimes (A_1 \oplus E'_2) = A_1 \oplus E'_1 \oplus E \oplus E'_3 \oplus E'_2. \quad (\text{S10})$$

The states transforming according to the IrRep E correspond to both electrons and both holes residing in the same valley, similarly the E'_3 IrRep corresponds to both electrons residing in the same valley and both holes residing in the opposite valley to the electrons, and finally E'_2 corresponds to both electrons residing in opposite valleys, and both holes residing in the same valley. As these three cases require one of the holes to reside in the lower spin-orbit split band in order for the biexciton to be bound, we do not consider these states. Of particular interest is the A_1 representation corresponding to both electrons and both holes residing in opposite valleys. Including the spin projections this corresponds to the following biexciton state, $B_{\downarrow K, \uparrow K'}^{\uparrow K, \downarrow K'}$ which is the semi-dark (due to momentum conservation) ground state singlet biexciton, and $B_{\uparrow K, \downarrow K'}^{\uparrow K, \downarrow K'}$ which is the excited bright state singlet biexciton. As the two states transform according to the same IrRep A_1 , they can also be mixed by the electron-electron intervalley scattering process as in the trions case. The biexciton triplet states are given by $B_{\uparrow K, \uparrow K'}^{\uparrow K, \downarrow K'}$ and $B_{\downarrow K, \downarrow K'}^{\uparrow K, \downarrow K'}$ both being optically bright. The biexciton states transforming according to the E_1 IrRep are bright having both electrons in the same valley and both holes in opposite valleys, $[B_{\uparrow K, \downarrow K}^{\uparrow K, \downarrow K'} ; B_{\uparrow K', \downarrow K'}^{\uparrow K, \downarrow K'}]$.

Table S3: Group theory classification.

Summary of the group theory classification of excitonic complexes, X -excitons, T -trions, and B - Biexcitons, in Tungsten dichalcogenides according to the irreducible representations of the extended point group C_{3v}'' . The last column indicates the corresponding symbol used in the main text.

	IrRep	States	Bright	Dark	Exciton or complex (see Fig. 2)	
X	E	$[X_{\downarrow K}^{\uparrow K}; X_{\uparrow K'}^{\downarrow K'}]$		✓	X_d	
		$[X_{\uparrow K}^{\uparrow K}; X_{\downarrow K'}^{\downarrow K'}]$	✓		X_b	
	E'_3	$[X_{\uparrow K'}^{\uparrow K}; X_{\downarrow K}^{\downarrow K'}]$		✓	X_d	
		$[X_{\downarrow K'}^{\uparrow K}; X_{\uparrow K}^{\downarrow K'}]$		✓		
T	E'_2	$[T_{\downarrow K, \uparrow K'}^{\uparrow K}; T_{\downarrow K, \uparrow K'}^{\downarrow K'}]$	} mix		✓	T_{sd}
		$[T_{\uparrow K, \downarrow K'}^{\uparrow K}; T_{\uparrow K, \downarrow K'}^{\downarrow K'}]$		✓		T^*
	E	$[T_{\uparrow K, \uparrow K'}^{\uparrow K}; T_{\downarrow K, \downarrow K'}^{\downarrow K'}]$	✓		T	
		$[T_{\downarrow K, \downarrow K'}^{\uparrow K}; T_{\uparrow K, \uparrow K'}^{\downarrow K'}]$		✓	–	
	E	$[T_{\uparrow K, \downarrow K}^{\uparrow K}; T_{\uparrow K', \downarrow K'}^{\downarrow K'}]$	✓		T	
	E'_3	$[T_{\uparrow K, \downarrow K}^{\downarrow K'}; T_{\uparrow K', \downarrow K}^{\uparrow K}]$		✓	–	
B	A_1	$B_{\downarrow K, \uparrow K'}^{\uparrow K, \downarrow K'}$	} mix		✓	B_{sd}
		$B_{\uparrow K, \downarrow K'}^{\uparrow K, \downarrow K'}$		✓		B^*
		$B_{\uparrow K, \uparrow K'}^{\uparrow K, \downarrow K'}$		✓		B
	E'_1	$B_{\downarrow K, \downarrow K'}^{\uparrow K, \downarrow K'}$	✓		B	
		$[B_{\uparrow K, \downarrow K}^{\uparrow K, \downarrow K'}; B_{\uparrow K', \downarrow K'}^{\uparrow K, \downarrow K'}]$	✓		B	

S2 Model calculations of the intervalley scattering matrix element

S2.1 Ab initio density functional theory

In the DFT calculations the wave functions were obtained in the local density approximation, using a plane-wave basis of 600 eV cutoff energy and a k-point grid of 12×12 in the 2D Brillouin zone. We used the VASP² code for these calculations, which employs periodic boundary conditions in three dimensions even for 2D materials; for this reason we used a large inter-layer distance of 20 Å to mimic the limit of an isolated monolayer. The form factor was calculated by post-processing the DFT wave functions, simply taking the matrix element of the bare Coulomb interaction between the initial and final states of the scattering process. In the calculation of this matrix element we neglected spin-orbit coupling.

The form factor was calculated in reciprocal space by Fourier transforming Eq. (2) in the main text, leading to a summation on the grid of reciprocal lattice vectors. This technique is sensitive to the plane-wave cutoff energy. We have therefore tested the sensitivity of the form factor to the cutoff energy by calculating it for WS₂ with an extremely reduced cutoff of 100 eV and an increased cutoff of 900 eV. We found that reducing the cutoff reduces the form factor by 10 %, while increasing the cutoff increases the form factor by 3 %.

Convergence of the calculation was also tested for the inter-layer separation. We found that

decreasing the separation to 15 Å only changes the form factors by less than 1 %.

In Fig. S1 we show the DFT calculated band structure for WS_2 and WSe_2 , showing the band edges at the K point and the spin-orbit splitting. In Tables S4 and S5 we list the DFT obtained orbital decomposition of the electron states at the K/K' points in the conduction and valence bands demonstrating the dominance of the transition metal d orbitals.

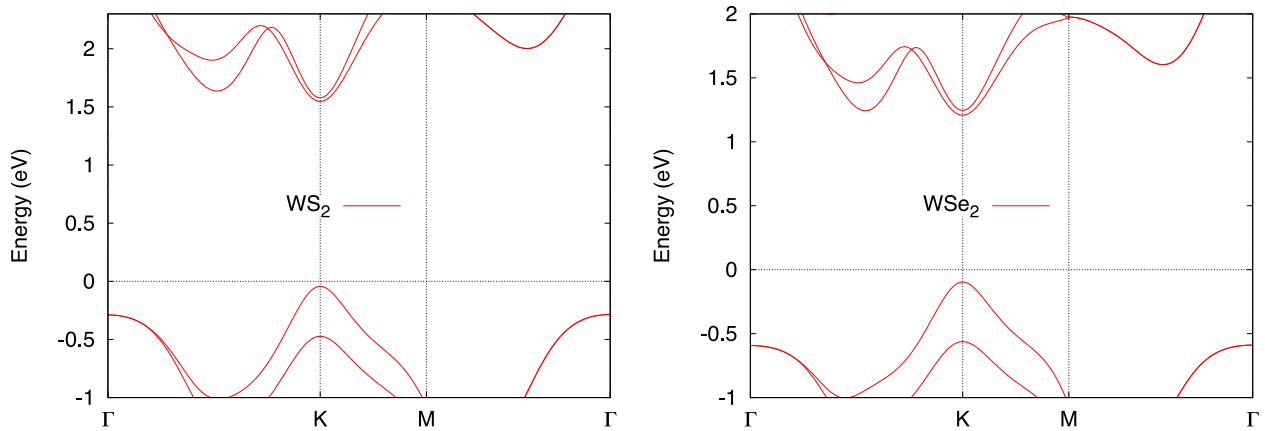


Figure S1 | DFT calculated band structure of WX_2 .

Table S4 | DFT calculated orbital decomposition at the K/K' point in WS_2 .

band	W - $5d_{z^2}$	W - $5d_{x^2-y^2}$	W - $5d_{xy}$	W - $6s$	S - p_x	S - p_y
c	86.9%	0	0	7.8%	2.6%	2.6%
v	0	39.5%	39.5%	0	10.2%	10.2%

Table S5 | DFT calculated orbital decomposition at the K/K' point in WSe_2 .

band	W - $5d_{z^2}$	W - $5d_{x^2-y^2}$	W - $5d_{xy}$	W - $6s$	Se - p_x	Se - p_y
c	85.9%	0	0	8.1%	2.2%	2.2%
v	0	40.1%	40.1%	0	9.2%	9.2%

S2.2 Tight-binding model

In the tight binding model, the Bloch wave function of the conduction band electrons at the K point, using only the transition metal d -orbital is given by

$$\Psi(\vec{r}) = \frac{C}{\sqrt{N}} \sum_i e^{i\vec{k}\cdot\vec{R}_i} \phi(\vec{r} - \vec{R}_i), \quad (\text{S11})$$

where N is the number of unit cells, \vec{R}_i is the lattice vector coinciding with the transition metal atoms positions, and C is the weight of the $5d_{z^2}$ orbital ϕ centred on \vec{R}_i . The value of C is obtained from the orbital decomposition given in Tables S4, S5 for WS_2 and WSe_2 , respectively. The 3D coulomb matrix element is given by

$$M = e^2 \int \frac{d^3\vec{r}_1 d^3\vec{r}_2}{|\vec{r}_2 - \vec{r}_1|} \Psi^*(\vec{r}_1) \Psi^*(\vec{r}_2) \Psi(\vec{r}_1) \Psi(\vec{r}_2). \quad (\text{S12})$$

Plugging in the Bloch wave function and using the two-centre approximation for the electron-electron Coulomb interaction we get

$$M = e^2 |C|^4 \sum_{\vec{R}} e^{i\vec{k}\cdot\vec{R}} \int d^3\vec{r}_1 d^3\vec{r}_2 \frac{|\phi(\vec{r}_1)|^2 |\phi(\vec{r}_2)|^2}{|\vec{r}_2 - \vec{r}_1 + \vec{R}|}, \quad (\text{S13})$$

where the summation is over the lattice sites $\vec{R} = l\vec{a}_1 + n\vec{a}_2$, where $\vec{a}_1 = a_0(1, 0)$, and $\vec{a}_2 = \frac{a_0}{2}(1, \sqrt{3})$ are the lattice primitive vectors, a_0 is the lattice constant, and l, n are integers. Finally, the matrix element is related to the dimensionless parameter χ through the intervalley interaction Hamiltonian giving,

$$\chi = \frac{m_c}{m} \frac{A}{a_B} |C|^4 \sum_{\vec{R}} e^{i\vec{K}\cdot\vec{R}} \int d^3\vec{r}_1 d^3\vec{r}_2 \frac{|\phi(\vec{r}_1)|^2 |\phi(\vec{r}_2)|^2}{|\vec{r}_2 - \vec{r}_1 + \vec{R}|}, \quad (\text{S14})$$

where m_c is the c -band electron mass, m is the free electron mass, A is the unit cell area, and a_B is the Bohr radius.

For the atomic orbital entering into the Coulomb matrix element we use the Roothaan-Hartree-Fock (RHF) atomic orbitals^{6,7} which consist of a linear combination of Slater-type orbitals,

$$\phi_{nlm}(\vec{r}) = Y_m^l(\theta, \phi) \sum_j C_j S_j(r) = Y_m^l(\theta, \phi) R_{nl}(r), \quad (\text{S15})$$

where n, l , and m are the principle, azimuthal and magnetic quantum numbers, and $Y_m^l(\theta, \phi)$ are the spherical harmonics. The Slater-type radial orbital $S(r)$ has the general form

$$S(r) = N_s r^{n-1} e^{-Zr}, \quad (\text{S16})$$

here $N_s = \frac{(2Z)^{n+1/2}}{\sqrt{(2n)!}}$ is a normalization constant, and Z is the orbital exponent. Using the tables in

Ref. [7] we construct the Tungsten $5d_{z^2}$ orbital, with the radial part given by (in atomic units)

$$\begin{aligned}
R_{5d}(r) = & -1070.29e^{-29.4731r}r^2 - 1297.24e^{-18.363r}r^2 \\
& + 1192.26e^{-12.073r}r^3 + 239.385e^{-7.9781r}r^3 \\
& - 56.2785e^{-5.19312r}r^4 - 7.74766e^{-3.14551r}r^4 \\
& - 0.18956e^{-1.79159r}r^4,
\end{aligned} \tag{S17}$$

and the angular part is $Y_0^2(\theta, \phi) = \frac{\sqrt{5}}{4\pi}(3 \cos^2 \theta - 1)$.

We separate the calculation of the matrix element into two parts, first taking $\vec{R} = 0$ giving the on-site contribution, and then allowing for $\vec{R} \neq 0$. For the on-site contribution with $\vec{R} = 0$, we expand the Coulomb potential in spherical harmonics

$$\frac{1}{|\vec{r}_2 - \vec{r}_1|} = \sum_{l=0}^{\infty} \frac{r_{<}^l}{r_{>}^{l+1}} \sum_{m=-l}^{m=l} \frac{4\pi}{2l+1} Y_m^{l*}(\theta', \phi') Y_m^l(\theta, \phi), \tag{S18}$$

which allows to separate the radial and angular integrations. The angular integration consists of products of three spherical harmonics which can be written in terms of Wigner 3j-symbols,

$$\begin{aligned}
& \int Y_{m_1}^{l_1}(\theta, \phi) Y_{m_2}^{l_2}(\theta, \phi) Y_{m_3}^{l_3}(\theta, \phi) \sin \theta d\theta d\phi \\
& = \sqrt{\frac{(2l_1+1)(2l_2+1)(2l_3+1)}{4\pi}} \begin{pmatrix} l_1 & l_2 & l_3 \\ 0 & 0 & 0 \end{pmatrix} \begin{pmatrix} l_1 & l_2 & l_3 \\ m_1 & m_2 & m_3 \end{pmatrix}.
\end{aligned} \tag{S19}$$

The Wigner 3j-symbols impose selection rules on the possible values of the different angular momentum quantum numbers, thus reducing the number of terms in the sum and the number of integrations needed. In particular we must have, $m_1 + m_2 + m_3 = 0$, $|m_i| < l_i$, and $|l_1 - l_2| \leq l_3 \leq l_1 + l_2$.

For the case of non-zero \vec{R} , since the wave functions have a typical spread smaller than the lattice constant, we use the following expansion^{8,9} valid for $|\vec{r}_1 + \vec{r}_2| < R$,

$$\begin{aligned}
\frac{1}{|\vec{r}_2 - \vec{r}_1 + \vec{R}|} &= \sum_{l_a, l_b=0}^{\infty} R^{-(l_a+l_b+1)} r_1^{l_a} r_2^{l_b} V_{l_a, l_b}; \tag{S20} \\
V_{l_a, l_b} &= (4\pi)^{3/2} (-1)^{l_b} \binom{2(l_a + l_b)}{2l_a}^{1/2} \\
&\times [(2l_a + 1)(2l_b + 1)(2(l_a + l_b) + 1)]^{-1/2} \\
&\times \sum_{M=-(l_a+l_b)}^{l_a+l_b} (-1)^M Y_{-M}^L(\hat{R}) [Y^{l_a}(\hat{r}_1) \otimes Y^{l_b}(\hat{r}_2)]_M^{l_a+l_b}; \\
[Y^{l_a}(\hat{r}_1) \otimes Y^{l_b}(\hat{r}_2)]_M^{l_a+l_b} &= \sum_{m_a=-l_a}^{l_a} \sum_{m_b=-l_b}^{l_b} Y_{m_a}^{l_a}(\hat{r}_1) Y_{m_b}^{l_b}(\hat{r}_2) \\
&\times \langle l_a m_a; l_b m_b | (l_a + l_b) M \rangle.
\end{aligned}$$

In Fig. S2 we show the convergence of the summation using both the detailed analytical method and a Monte Carlo calculation of the integral in Eq. (S14), showing that both methods converge to the same value for the dimensionless matrix element χ .

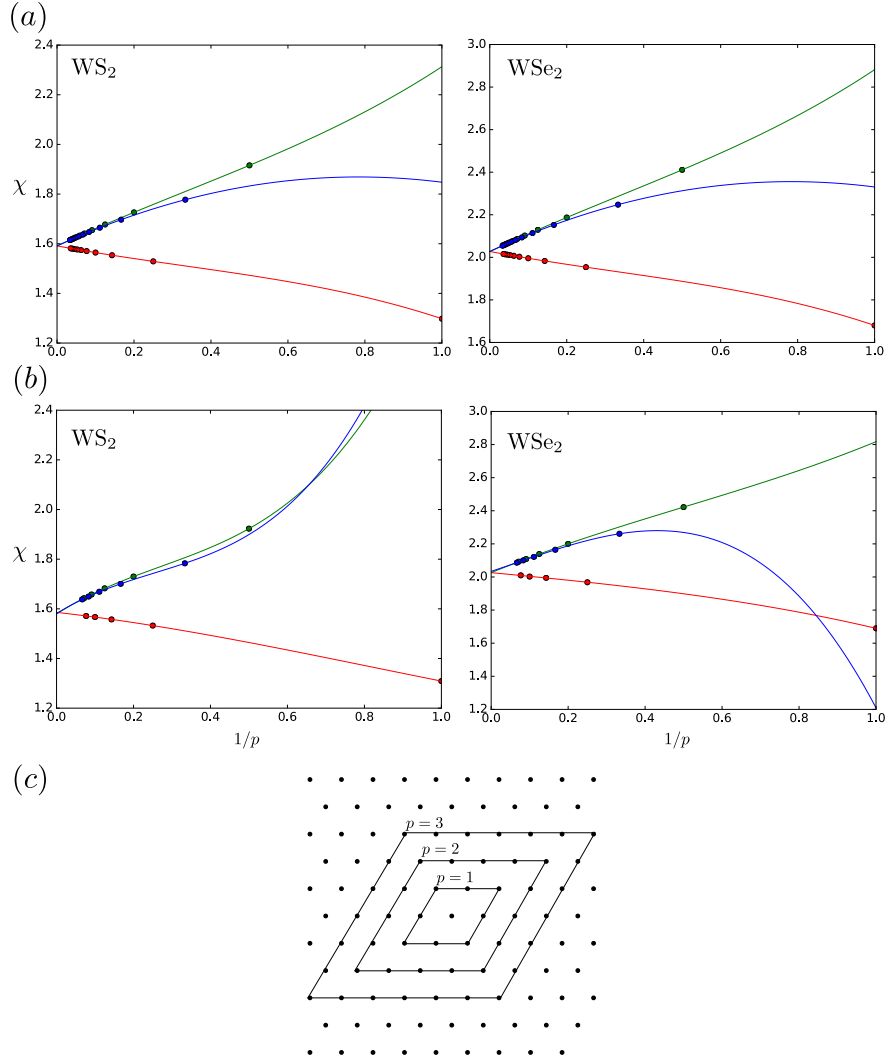


Figure S2 | Convergence of the intervalley scattering matrix element calculation.

(a) Analytical calculation of the matrix element as a function of the inverse number of lattice points in the summation. (b) Monte Carlo calculation results. We fit the points to third order polynomials and extract the value for $1/p \rightarrow 0$ corresponding to summation over an infinite lattice. The data points are separated into three sequences with a period of 3, all converging to the same point. This behaviour of the sum is attributed to the phase factor in the summation involving the \vec{K} vector, and to the rhombic unit cell used in the summation. (c) Sketch of the rhombic unit cell used for the summation over the triangular lattice points for increasing values of p .

1. Gui-Bin Liu, Di Xiao, Yugui Yao, Xiaodong Xu, and Wang Yao. Electronic structures and theoretical modelling of two-dimensional group-vib transition metal dichalcogenides. *Chem. Soc. Rev.*, 44:2643–2663, 2015.
2. Andor Kormanyos, Guido Burkard, Martin Gmitra, Jaroslav Fabian, Viktor Zolyomi, Neil D Drummond, and Vladimir Fal’ko. k,p theory for two-dimensional transition metal dichalcogenide semiconductors. *2D Materials*, 2(2):022001, 2015.
3. Mark Danovich, Viktor Zólyomi, Vladimir I Fal’ko, and Igor L Aleiner. Auger recombination of dark excitons in ws 2 and wse 2 monolayers. *2D Materials*, 3(3):035011, 2016.
4. Basko, D. M. Theory of resonant multiphonon Raman scattering in graphene. *Phys. Rev. B*, 78:125418, Sep 2008.
5. Bogdan Ganchev, Neil Drummond, Igor Aleiner, and Vladimir Fal’ko. Three-particle complexes in two-dimensional semiconductors. *Phys. Rev. Lett.*, 114:107401, Mar 2015.
6. Yue Wu, Qingjun Tong, Gui-Bin Liu, Hongyi Yu, and Wang Yao. Spin-valley qubit in nanostructures of monolayer semiconductors: Optical control and hyperfine interaction. *Phys. Rev. B*, 93:045313, Jan 2016.
7. A. D. McLean and R. S. McLean. Roothaan–hartree–fock atomic wave functions slater basis-set expansions for z=55–92. *Atomic Data and Nuclear Data Tables*, 26(3–4):197–381, 1981.
8. Iliia A. Solov’yov, Alexander V. Yakubovich, Andrey V. Solov’yov, and Walter Greiner. Two-center-multipole expansion method: Application to macromolecular systems. *Phys. Rev. E*, 75:051912, May 2007.

9. Arrighini Paolo. *Intermolecular Forces and Their Evaluation by Perturbation Theory*, volume 25 of *Lecture Notes in Chemistry*. Springer, Berlin, 1981.
10. G. Kresse and J. Furthmüller. Efficient iterative schemes for *ab initio* total-energy calculations using a plane-wave basis set. *Phys. Rev. B*, 54:11169–11186, Oct 1996.